CASSON FLUID FLOW WITH ARRHENIOUS FUNCTION OVER AN EXPONENTIAL STRETCHING SHEET

[1]MOHAMMED I. B. S., [2]OLAYIWOLA R.O., [2]A. A. MOHAMMED AND [2]N. NYOR
[1]*Department of Mathematics, Federal Polytechnic Bida, Nigeria.*
[2]*Department of Mathematics, Federal University of Technology Minna, Nigeria.*

Abstract
This paper transformed the model equations of casson fluid flow with Arrhenious function over an exponential stretching sheet from non-linear partial differential equations (PDE) to ordinary differential equations (ODE) using suitable similarity transformation. The transformed equations were solved using iteration perturbation method. The graphical illustrations were provided and it was observed that velocity profile decreases with increase in casson, magnetic, permeability and porosity parameters while increase in ratio parameter, thermal and solutal grashof numbers enhance the velocity profiles, Soret number increse the concentration profile while chemical reaction parameter, activation energy parameter and schmidtl number decrease the concentration profile. Increase in magnetic parameter, radiative parameter, heat source, dufour number, chemical reaction and activation energy parameters enhance the temperature profile while increase in prandtl number decreases the temperature profile.

Keywords: *Activation energy, Casson fluid, Chemical reaction, Stretching sheet, Non-Newtonian,*

Introduction
A fluid in which the viscous stresses arising from its flow at every point are linearly proportional to the rate of change in its deformation over time is called Newtonian fluid. This means that in a Newtonian fluid, the relationship between the shear stress and the shear rate are linear with the

proportionality constant referred to as the coefficient of viscosity. On the other hand, a fluid whose flow properties are different in any way from that of the Newtonian fluid is called a non-Newtonian fluid. Casson fluid is classified as a non-Newtonian fluid due to its rheological characteristics. These characteristics show shear stress-strain relationships that are significantly different from Newtonian fluid. Many researchers have developed and studied the transport properties of Casson fluid over the last few decades. Pushapalata *et al.* (2016) investigated the unsteady free convective flow of a casson fluid bounded by a moving vertical plate in a rotating system. Sarojamma *et al.* (2014) analyzed the flow, heat and mass transfer characteristics of a MHD casson fluid in a parallel plate channel with stretching walls subject to a uniform transverse magnetic field. Kushpalalata *et al.* (2017) analyzed the effects of cross diffusion on casson fluid over an unsteady stretching surface with boundary effects.

Maleque (2016) investigated an exothermic/endothermic binary chemical reaction on unsteady MHD non-Newtonian casson fluid flow with heat and mass transfer past a flat porous plate. Maleque (2013) investigated the effects of exothermic/endothermic chemical reaction with Arrhenius activation energy on MHD free convection mass transfer flow in presence of thermal radiation. Prakash *et al.* (2016) examined the thermal and solutal boundary layer in incompressible, laminar flow over an exponentially stretching sheet with variable temperature and concentration in the presence of chemical reaction and thermal radiation. Charankumar *et al.* (2016) examined chemical reaction and Soret effects on casson MHD fluid flow over a vertical plate with heat source/sink. The problem was solved numerically using perturbation technique for the velocity, the temperature and the concentration species.

Kumar and Gangadhar (2015) investigated the interactions of MHD stagnation point of electrically conducting non-Newtonian casson fluid and heat transfer towards a stretching sheet in the presence of viscous dissipation, momentum and thermal slip flow. Saidulu and Lakshmi (2016) described the boundary layer flow of non-Newtonian Casson fluid accompanied by heat and mass transfer towards a porous exponentially stretching sheet with velocity slip and thermal slip conditions in presence of thermal radiation, suction/blowing, viscous dissipation, heat source/sink and chemical reaction effects. Vedavathi *et al.* (2016) examined chemical reaction, radiation and dufour effects on Casson MHD fluid flow over a vertical plate with heat source/sink and the problem was solved numerically using perturbation technique. Gireesha *et al.* (2016)

examined the similarity solution to the problem of two - dimensional boundary layer flow, heat and mass transfer of non-Newtonian Casson fluid over a porous stretching surface. Kirubhashankar *et al.* (2015) investigated Casson fluid flow and heat transfer over an unsteady porous Stretching surface. Hussanan *et al.* (2016) investigated the effects of Newtonian heating and inclined magnetic field on two-dimensional flow of a Casson fluid over a stretching sheet. This paper presents a steady three dimensional casson fluid flow model with Arrhenious function over an exponential stretching sheet.

Model Formulation

We consider three dimensional (3D) steady incompressible flows past a non-isothermal exponentially stretching sheet. The sheet is stretched along the xy plane, while the fluid is placed along the z - axis; the uniform magnetic field is applied in z - direction that is perpendicular to the flow direction. Here, we assumed that the sheet was stretched with velocities $U_w = U_0 e^{\frac{x+y}{L}}$ and $V_w = V_0 e^{\frac{x+y}{L}}$ along the xy -plane respectively, $T_w = T_0 e^{\frac{x+y}{L}}$ and $C_w = C_0 e^{\frac{x+y}{L}}$. A heat source/sink placed within the flow to allow for heat generation or absorption effects.

The rheological equation of state for an isotropic flow of casson fluid as stated by (Pushpalata et al. 2017) can be expressed as:

$$\tau_{ij} = \begin{cases} 2\left(\mu_B + \frac{p_z}{\sqrt{2\pi}}\right)e_{ij}, \pi > \pi_c \\ 2\left(\mu_B + \frac{p_z}{\sqrt{2\pi_c}}\right)e_{ij}, \pi < \pi_c \end{cases}$$

(1)

In the above equation $\pi = e_{ij}e_{ij}$ and e_{ij} denotes the $(i,j)^{th}$ components of the deformation rate, π is the product of the deformation rate itself, π_c is the critical value of this product based on the non-Newtonian fluid model, μ_B is the plastic dynamic viscosity of the non-Newtonian fluid and p_z is the yield stress of the fluid. From (1), we obtain $\mu_B = \frac{1}{2}\frac{\tau_{ij}}{e_{ij}} - \frac{p_z}{\sqrt{2\pi}}$, $\upsilon = \frac{\mu_B}{\rho}$ and $\beta = \frac{\sqrt{2\pi_c}}{p_z}\mu_B$

The boundary layer equations of three-dimensional incompressible casson fluids flow are given as follows

$$\frac{\partial u}{\partial x} + \frac{\partial v}{\partial y} + \frac{\partial w}{\partial z} = 0 \tag{2}$$

$$u\frac{\partial u}{\partial x} + v\frac{\partial u}{\partial y} + w\frac{\partial u}{\partial z} = \upsilon\left(1+\frac{1}{\beta}\right)\left[\frac{\partial^2 u}{\partial z^2}\right] - \frac{\sigma B^2}{\rho}u - \frac{\upsilon}{K}u - \Gamma u^2 + g_g\beta_T\left(T-T_\infty\right) \\ + g_g\beta_c\left(C-C_\infty\right) \tag{3}$$

$$u\frac{\partial v}{\partial x} + v\frac{\partial v}{\partial y} + w\frac{\partial v}{\partial z} = \upsilon\left(1+\frac{1}{\beta}\right)\left[\frac{\partial^2 v}{\partial z^2}\right] - \frac{\sigma B^2}{\rho}v - \frac{\upsilon}{K}v - \Gamma v^2 \tag{4}$$

$$u\frac{\partial T}{\partial x} + v\frac{\partial T}{\partial y} + w\frac{\partial T}{\partial z} = \frac{k_h}{\rho c_p}\left[\frac{\partial^2 T}{\partial z^2}\right] + \frac{D_m k_T}{T_m c_S}\frac{\partial^2 C}{\partial z^2} + \frac{\sigma B^2}{\rho}\left(u^2+v^2\right) + \\ \frac{Q_1}{\rho c_p}\left(T-T_\infty\right) - \frac{1}{\rho c_p}\frac{\partial q_r}{\partial z} + \beta_{EE}k_r^2\left(T-T_\infty\right)^n.\left(C-C_\infty\right)e^{-\frac{E_a}{k\left(T-T_\infty\right)}} \tag{5}$$

$$u\frac{\partial C}{\partial x} + v\frac{\partial C}{\partial y} + w\frac{\partial C}{\partial z} = D_m\frac{\partial^2 C}{\partial z^2} + \frac{D_m k_T}{T_m}\frac{\partial^2 T}{\partial z^2} - k_r^2\left(T-T_\infty\right)^n.\left(C-C_\infty\right)e^{-\frac{E_a}{k\left(T-T_\infty\right)}} \tag{6}$$

Subject to the initial and boundary conditions:

$$\left. \begin{array}{l} u = U_w, v = V_w, T = T_w, C = C_w \; at \; z = 0 \\ u \to 0, v \to 0, T \to T_\infty, C \to C_\infty \; as \; z \to \infty \end{array} \right\} \tag{7}$$

Where , u, v and w are the velocity component in the direction of x, y and z respectively, β is the casson fluid parameter, υ is the kinematic viscosity, B is the magnetic induction, B_0 is constant, K and Γ are permeability and the inertia coefficient of porous medium, T is temperature, C is the concentration of the fluid, β_T and β_C are the coefficient of volume expansion for temperature and concentration differences respectively, β_{C_0} and β_{T_0} are constants, Q_1 is heat source, Q_0 is constant, k_T is the thermal diffusivity ratio, α_h is the thermal diffusivity, δ is the density of the fluid, g_g is acceleration due to gravity, σ is the electrical conductivity, k_h is the thermal conductivity, c_p is the specific heat capacity at constant pressure, c_S is the concentration susceptibility, T_∞ is the free stream temperature, T_m

is the mean fluid temperature, D_m is the coefficient of mass diffusivity, k_r is the chemical reaction rate, k_{r_0} is constant, $\beta_{EE}(=\pm 1)$ is the exothermic/endothermic parameter, $(T-T_\infty)^n.(C-C_\infty)e^{-\frac{E_a}{k(T-T_\infty)}}$ is the Arrhenius function where η is the dimensionless exponent fitted rate constant typically lie in the range $-1 < n < 1$, E_a is the activation energy, k is the Boltzmann constant k_0 is constant and the radiative heat flux q_r is

described by Roseland approximation such that $q_r = -\frac{4\sigma_1}{3k_1}\frac{\partial(T^4)}{\partial z}$ where σ_1 and k_1 are the Stefan Boltzmann constant and mean absorption coefficient respectively.

Method of Solution
Using the similarity variables:

$$\eta = \sqrt{\frac{U_0}{2\upsilon L}}e^{\frac{x+y}{2L}}z, u = U_0 e^{\frac{x+y}{L}}f'(\eta), v = U_0 e^{\frac{x+y}{L}}g'(\eta), T = T_\infty + T_0 e^{\frac{x+y}{L}}\theta(\eta), C = C_\infty + C_0 e^{\frac{x+y}{L}}\phi(\eta),$$

$$\left.k_r = k_{r_0}e^{\frac{x+y}{2L}}, K = \frac{1}{K_0 e^{\frac{x+y}{L}}}, B = B_0 e^{\frac{x+y}{2L}}, k = \frac{k_0}{e^{\frac{x+y}{L}}}, Q_1 = Q_0 e^{\frac{x+y}{L}}, \beta_T = \beta_{T_0}e^{\frac{x+y}{L}}, \beta_C = \beta_{C_0}e^{\frac{x+y}{L}}\right\}$$

(8)

The transformed equations together with the boundary conditions are:

$$b_1 f''' + (f + \eta f' + g + \eta g')f'' - 2(f' + g')\left(f' + \frac{\eta}{2}f''\right) - b_2 f' - \Lambda f'^2 + G_{r_\theta}\theta + G_{r_\phi}\phi = 0$$

(9)

$$b_1 g''' + (f + \eta f' + g + \eta g')g'' - 2(f' + g')\left(g' + \frac{\eta}{2}g''\right) - b_2 g' - \Lambda g'^2 = 0$$

(10)

$$\frac{1}{P_r}\theta'' + \frac{R}{P_r}\theta'' + (f + \eta f' + g + \eta g')\theta' - 2(f' + g')\left(\theta + \frac{\eta}{2}\theta'\right) + M(f'^2 + g'^2)$$

$$+ Q_h\theta + \delta\phi e^{-\frac{\varepsilon}{\theta}} + S_r\phi'' = 0$$

(11)

$$\frac{1}{S_c}\phi'' + D_u\theta'' + (f + \eta f' + g + \eta g')\phi' - 2(f' + g')\left(\phi + \frac{\eta}{2}\phi'\right) - \delta\phi e^{-\frac{\varepsilon}{\theta}} = 0$$

(12)

$$f(0)=0, \quad g(0)=0, \; f'(0)=1, \quad g'(0)=\alpha, \quad \theta(0)=1, \quad \phi(0)=1 \;\Bigg\}$$
$$f' \to 0 \; as \; \eta \to \infty, \; g' \to 0 \; as \; \eta \to \infty, \; \theta \to 0 \; as \; \eta \to \infty, \; \phi \to 0 \; as \; \eta \to \infty \Bigg\} \tag{13}$$

Where

$$G_{r_\theta} = \frac{2Lg\beta_{T_0}T_0}{U_0^2}, G_{r_\phi} = \frac{2Lg\beta_{C_0}C_0}{U_0^2}, M = \frac{2L\sigma B_0^2}{\rho U_0}, \alpha_h = \frac{k_h}{\rho c_p}, K_p = \frac{2L\upsilon K_0}{U_0}, \Lambda = 2L\Gamma,$$

$$S_r = \frac{D_m k_T}{T_m}\frac{C_0}{\upsilon T_0}, \frac{1}{S_c} = \frac{D_m}{\upsilon}, \delta = \frac{2L\beta_{EE}k_{r_0}^2 C_0}{T_0 U_0}, Q_h = \frac{2LQ_0}{\rho c_p U_0}, R = \frac{16T_\infty^3\sigma_1}{3k_1 k_h}, \frac{1}{P_r} = \frac{k_h}{\rho c_p \upsilon}, D_u = \frac{D_m k_T}{T_m c_S}\frac{C_0}{\upsilon T_0}$$

Now, we begin with the initial approximate solution (Mohammed *et al.*, 2015; Olayiwola, 2016):

$$f_0 = \frac{1}{b}\left(1-e^{-b\eta}\right), \; g_0 = \frac{\alpha}{b}\left(1-e^{-b\eta}\right)\Bigg\} \tag{14}$$

Substituting the initial approximations (14) and embedding artificial parameter into (9) – (13) we have:

Order zero equations are:

$$b_1 f_0''' + b f_0'' = 0 \tag{15}$$

$$b_1 g_0''' + b g_0'' = 0 \tag{16}$$

$$\left(\frac{1+R}{p_r}\right)\theta_0'' + b\theta_0' = 0 \tag{17}$$

$$\frac{1}{S_c}\phi_0'' + b\phi_0' = 0 \tag{18}$$

Order one equations are:

$$b_1 f_1''' + b f_1'' + \left(\frac{1}{b}(1-e^{-b\eta})+\eta f_0' + \frac{\alpha}{b}(1-e^{-b\eta})+\eta g_0' - b\right)f_0'' - 2(f_0'+g_0')\left(f_0' + \frac{\eta}{2}f_0''\right)$$
$$- b_2 f_0' - \Lambda f_0'^2 + G_{r_\theta}\theta_0 + G_{r_\phi}\phi_0 = 0 \tag{19}$$

$$b_1 g_1''' + b g_1'' + \left(\frac{1}{b}(1-e^{-b\eta})+\eta f_0' + \frac{\alpha}{b}(1-e^{-b\eta})+\eta g_0' - b\right)g_0'' - 2(f_0'+g_0')\left(g_0' + \frac{\eta}{2}g_0''\right)$$
$$- b_2 g_0' - \Lambda g_0'^2 = 0 \tag{20}$$

$$\left(\frac{1+R}{P_r}\right)\theta_1'' + b\theta_1' + \left(\frac{1}{b}(1-e^{-b\eta})+\eta f_0' + \frac{\alpha}{b}(1-e^{-b\eta})+\eta g_0' - b\right)\theta_0' -$$
$$2(f_0'+g_0')\left(\theta_0 + \frac{\eta}{2}\theta_0'\right) + M\left(f_0'^2 + g_0'^2\right) + Q_h\theta_0 + \delta\phi_0 e^{-\frac{\varepsilon}{\theta_0}} + D_u\phi_0'' = 0 \tag{21}$$

$$\frac{1}{S_c}\phi_1'' + b\phi_1' + \left(\frac{1}{b}(1-e^{-b\eta})+\eta f_0' + \frac{\alpha}{b}(1-e^{-b\eta})+\eta g_0' - b\right)\phi_0' - 2(f_0'+g_0')\left(\phi_0 + \frac{\eta}{2}\phi_0'\right)$$
$$- \delta\phi_0 e^{-\frac{\varepsilon}{\theta_0}} + S_r\theta_0'' = 0 \tag{22}$$

Solving the resulting equations ((15) – (22)) as in (Mohammed et al. 2020), we obtain

$$f(\eta) = \frac{1}{q_2}\left(1 - e^{-q_2\eta}\right) + p\left(d_1\eta e^{-q_2\eta} + d_3 e^{-q_2\eta} - d_4 e^{-q_6\eta} - d_5 e^{-2q_2\eta} - d_6 e^{-q_3\eta} - d_7 e^{-bS_c\eta} + q_{16}\right)$$

$$g(\eta) = \frac{\alpha}{q_2}\left(1 - e^{-q_2\eta}\right) + p\left(q_{21}\eta e^{-q_2\eta} + q_{22} e^{-q_2\eta} - q_{25} e^{-2q_2\eta} + \frac{q_{26}}{q_2^2} e^{-q_2\eta} + q_{27}\right)$$

$$\theta(\eta) = e^{-q_3\eta} + p\left(q_{38} e^{-q_6\eta} - q_{36}\eta e^{-q_3\eta} - q_{37} e^{-q_3\eta} - q_{39} e^{-q_{32}\eta} + q_{40} e^{-2q_2\eta} + q_{41} e^{-bS_c\eta} + q_{42} e^{q_{34}\eta} - \frac{q_{43}}{q_3} e^{-q_3\eta}\right)$$

$$\phi(\eta) = e^{-bSc\eta} + p\left(q_{48} e^{-q_{53}\eta} - q_{45}\eta e^{-bS_c\eta} - q_{46} e^{-bS_c\eta} - q_{47} e^{-q_{52}\eta} - q_{49} e^{q_{54}\eta} + q_{50} e^{-2q_3\eta} - \frac{q_{51}}{bS_c} e^{-bS_c\eta}\right)$$

$$(23)$$

Where

$$b_1 = 1 + \frac{1}{\beta}, \quad b_2 = M + K_p, \quad q_2 = \frac{b}{b_1}, \quad q_3 = \frac{b}{b_5}, \quad b_5 = \frac{1+R}{p_r}, \quad q_4 = \frac{q_2}{b} + \alpha\frac{q_2}{b} - bq_2 + b_2,$$

$$q_5 = \left(\frac{q_2}{b} + \alpha\frac{q_2}{b}\right), q_6 = b + q_2, q_7 = 2 + 2\alpha + \Lambda, \quad q_9 = \frac{q_4}{b_1}, \quad q_{10} = \frac{q_5}{b_1(q_2 - q_6)}, \quad q_{11} = \frac{q_7}{b_1 q_2},$$

$$q_{13} = \frac{G_{r_\theta}}{b_1(q_2 - q_3)}, \quad q_{14} = \frac{G_{r_\phi}}{b_1(q_2 - bS_c)}, q_6 = b + q_2, \quad q_{17} = b_2\alpha + \frac{q_2\alpha}{b} + \alpha^2\frac{q_2}{b} - bq_2\alpha,$$

$$q_{18} = \left(\frac{q_2\alpha}{b} + \alpha^2\frac{q_2}{b}\right), \quad q_{20} = 2\alpha + 2\alpha^2 + \Lambda\alpha^2, \quad q_{21} = \frac{q_{17}}{q_2^2 b_1}, \quad q_{22} = 2\frac{q_{17}}{q_2^3 b_1} - \frac{q_{18}}{b_1 q_6^2(q_2 - q_6)},$$

$$q_{25} = \frac{q_{20}}{4q_2 b_1}, \quad q_{26} = \left(\frac{q_{18}}{b_1 q_6(q_2 - q_6)} - \frac{q_{17}}{q_2^2 b_1} + \frac{q_{20}}{2q_2 b_1} - \alpha\right)q_2, q_{27} = q_{25} - q_{22} - \frac{q_{26}}{q_2^2}$$

$$d_1 = \frac{q_9}{q_2^2}, \quad d_3 = 2\frac{q_9}{q_2^3} + \frac{q_{15}}{q_2^2}, d_4 = \frac{q_{10}}{q_2^2}, \quad d_5 = \frac{q_{11}}{4q_2^2}, \quad d_6 = \frac{q_{13}}{q_3^2}, \quad d_7 = \frac{q_{14}}{(bS_c)^2}$$

$$, q_{28} = b_3 - Q_h + \frac{q_3}{b} - bq_3 + \frac{\alpha q_3}{b}, \quad q_{30} = \left(\frac{q_3}{b} + \frac{\alpha q_3}{b}\right), q_{31} = 2 + 2\alpha, \quad q_{32} = q_2 + q_3,$$

$$q_{33} = M(1 + \alpha^2), \quad q_{34} = q_3 - bS_c, q_3 = \frac{b}{b_5}, q_{36} = \frac{q_{28}}{q_3 b_5}, q_{37} = \frac{q_{28}}{q_3^2 b_5}, q_{38} = \frac{q_{30}}{q_6 b_5(q_3 - q_6)},$$

$$q_{39} = \frac{q_{31}}{q_{32} b_5(q_3 - q_{32})}, \quad q_{40} = \frac{q_{33}}{2q_2 b_5(q_3 - 2q_2)}, \quad q_{41} = \left(\frac{\delta}{bS_c b_5(q_3 - bS_c)} + \frac{D_u(bS_c)^2}{bS_c b_5(q_3 - bS_c)}\right),$$

$$q_{42} = \frac{\delta\varepsilon}{q_{34} b_5(q_3 + q_{34})}, q_{43} = (q_{38} - q_{37} - q_{39} + q_{40} + q_{41} + q_{42} - 1)q_3, q_{45} = \left(-\frac{1}{b}\left(b_3 + \delta + S_c + \alpha S_c - b^2 S_c\right)\right),$$

$$q_{46} = \left(\frac{1}{b^2 S_c}\left(b_3 + \delta + S_c + \alpha S_c - b^2 S_c\right)\right), \quad q_{47} = \frac{S_c}{b(b + bS_c)}(S_c + \alpha S_c), q_{48} = \frac{S_c(2 + 2\alpha)}{q_2(q_2 + bS_c)},$$

$$q_{49} = \frac{\varepsilon\delta S_c}{q_3(q_3 - bS_c)}, q_{50} = \frac{S_r S_c q_3^2}{2q_3(bS_c - 2q_3)}, q_{51} = (q_{50} - q_{46} - q_{47} + q_{48} - q_{49} - 1)bS_c, q_{52} = b + bS_c,$$

$$q_{53} = (q_2 + bS_c), q_{54} = (q_3 - bS_c)$$

Results and discussion

The graphical illustrations for the steady state with Arrhenius chemical reaction are presented in in figures 4.1 to 4.22. The computations were done for different physical parameters which includes, casson parameter β, radiation parameter R, prandtl number P_r, schmidt number S_c, soret

number S_r, dufour number D_u, permeability parameter Λ, thermal grashof number G_{r_θ}, solutal grashof number G_{r_ϕ}, ratio parameter α, porosity parameter K_p, chemical reaction parameter δ, activation energy parameter ε, heat source Q_h and magnetic parameter M.
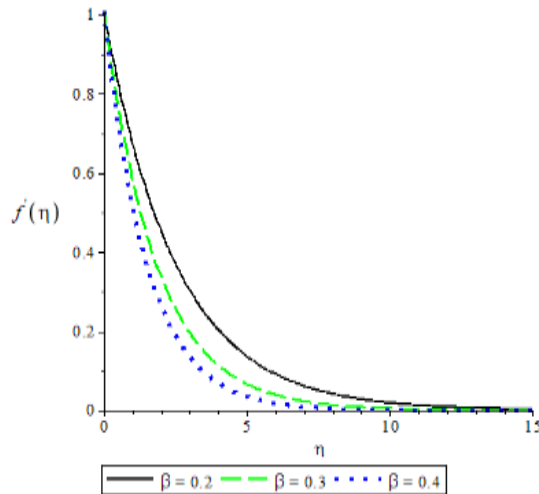
Figure 4.1: Effect of β on Velocity Profile $f'(\eta)$
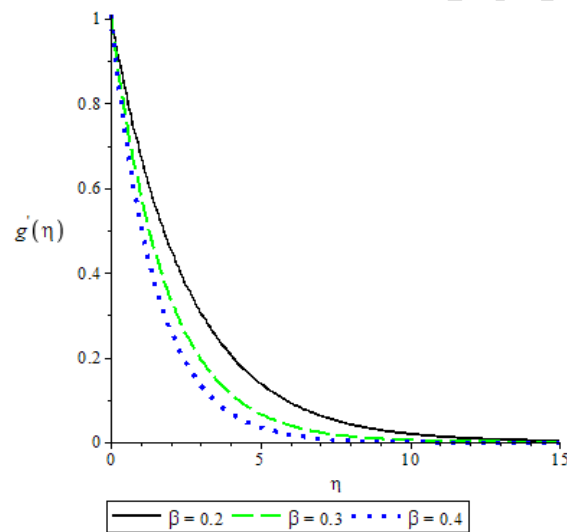
Figure 4.2: Effect of β on Velocity Profile $g'(\eta)$
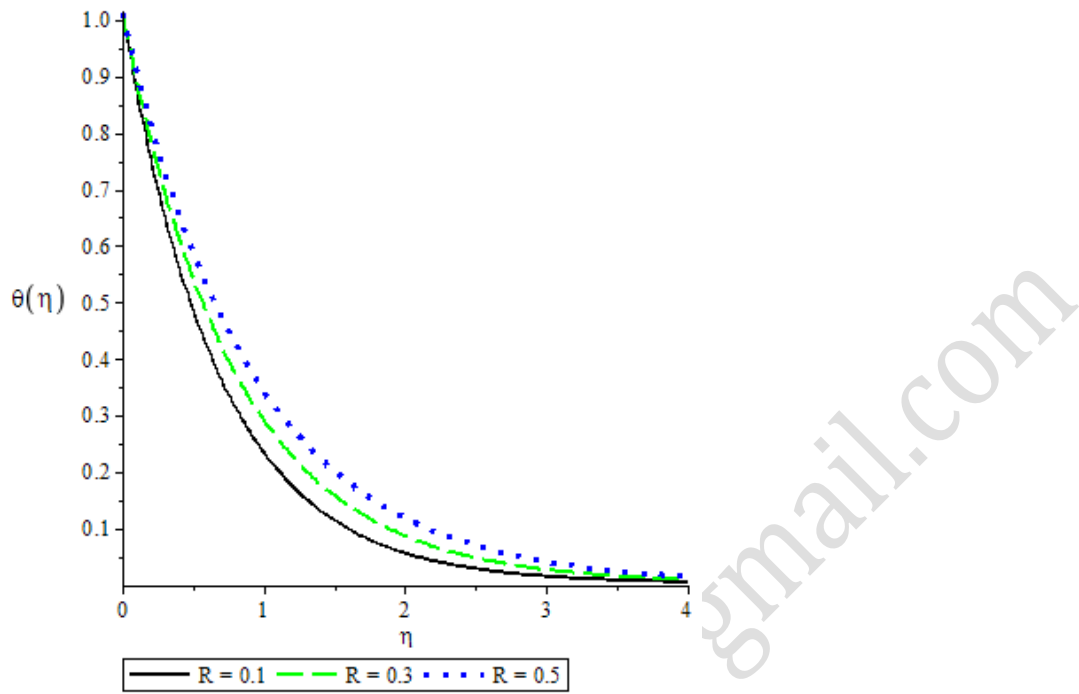
Figure 4.3: Effect of R on Temperature Profile $\theta(\eta)$
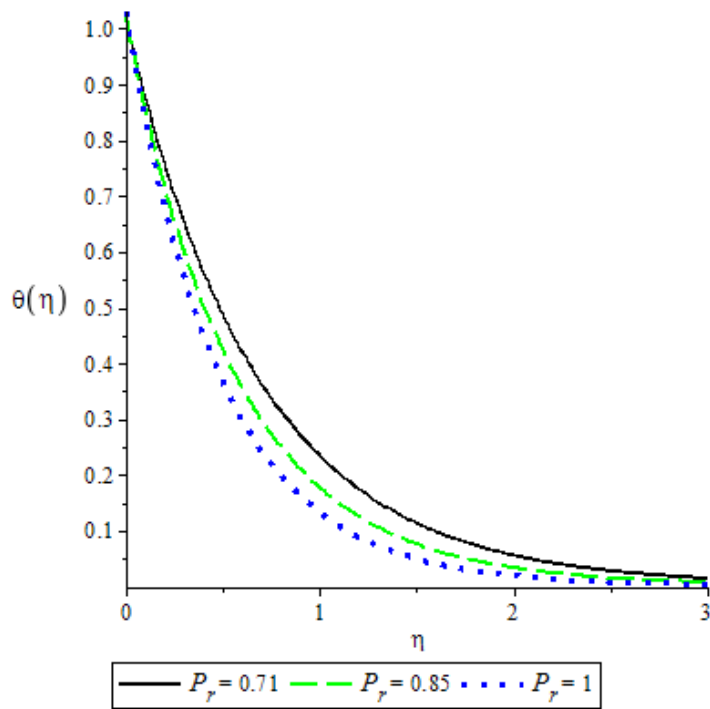
Figure 4.4: Effect of P_r on Temperature Profile $\theta(\eta)$
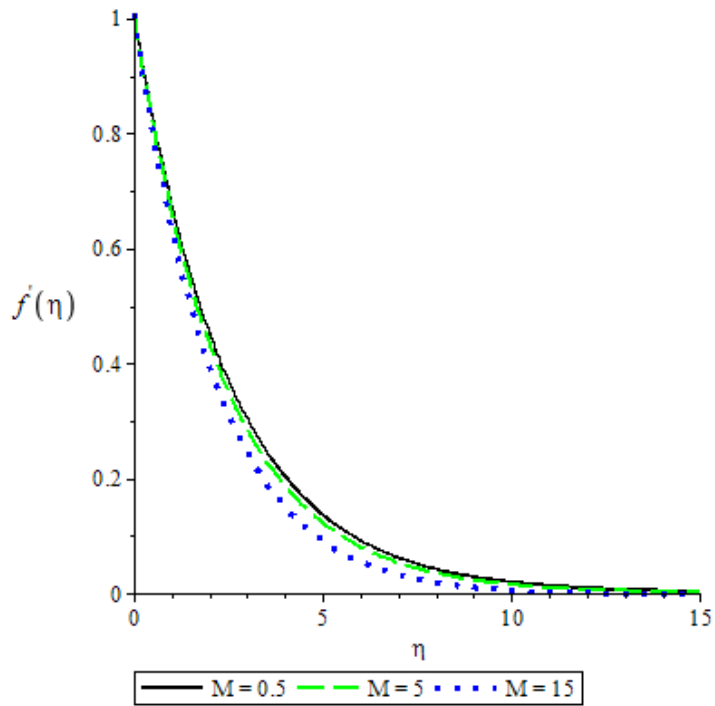
Figure 4.5: Effect of M on Velocity Profile $f'(\eta)$
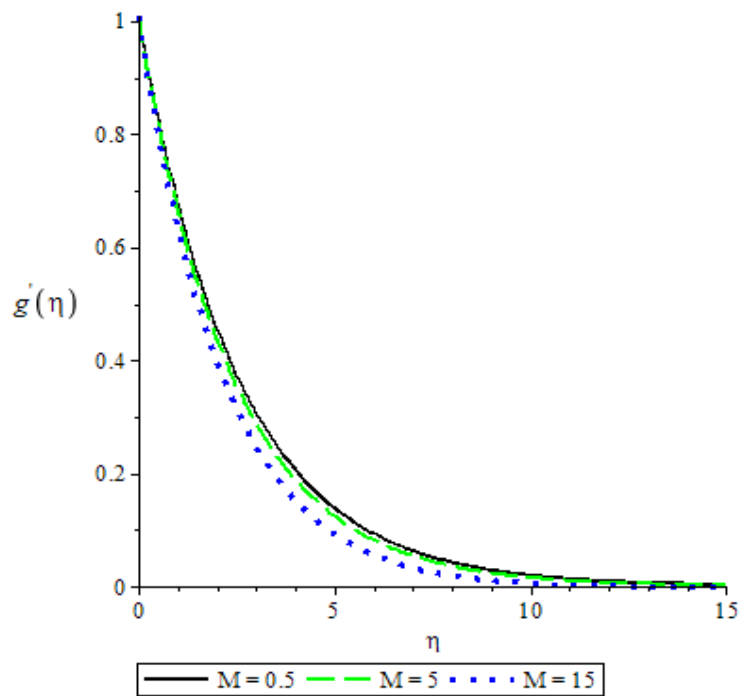
Figure 4.6: Effect of M on Velocity Profile $g'(\eta)$
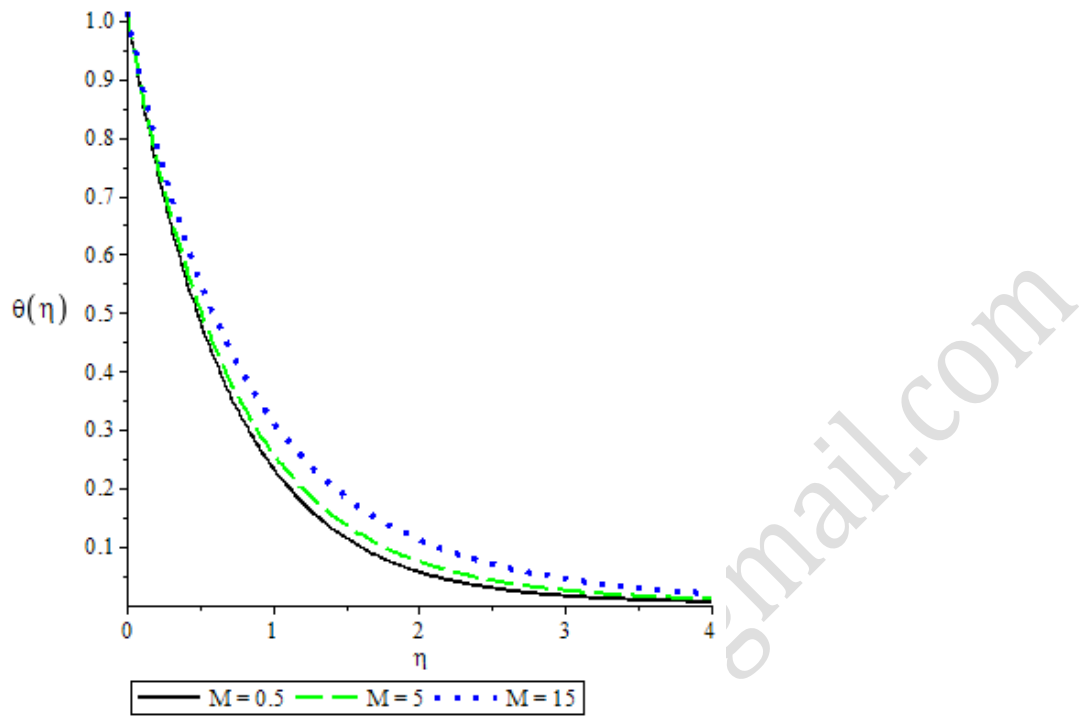
Figure 4.7: Effect of M on Temperature Profile $\theta(\eta)$
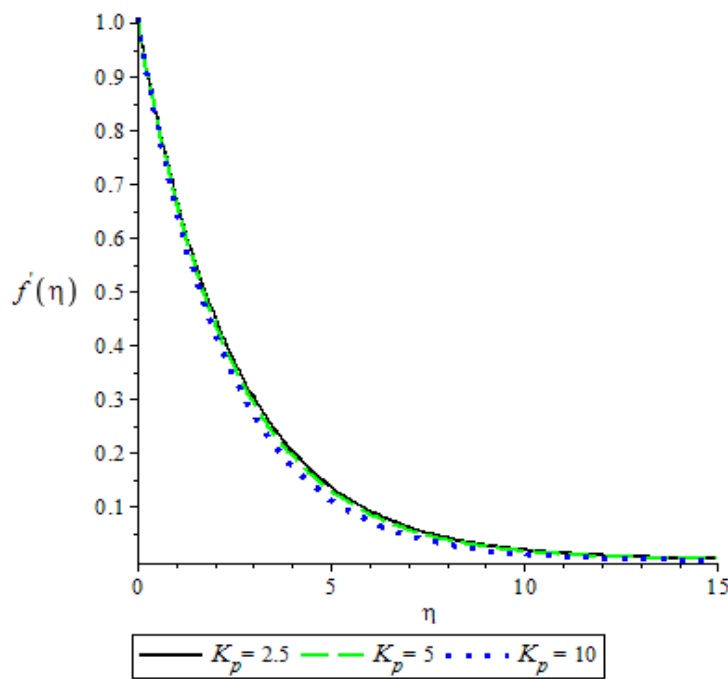
Figure 4.8: Effect of K_p on Velocity Profile $f'(\eta)$
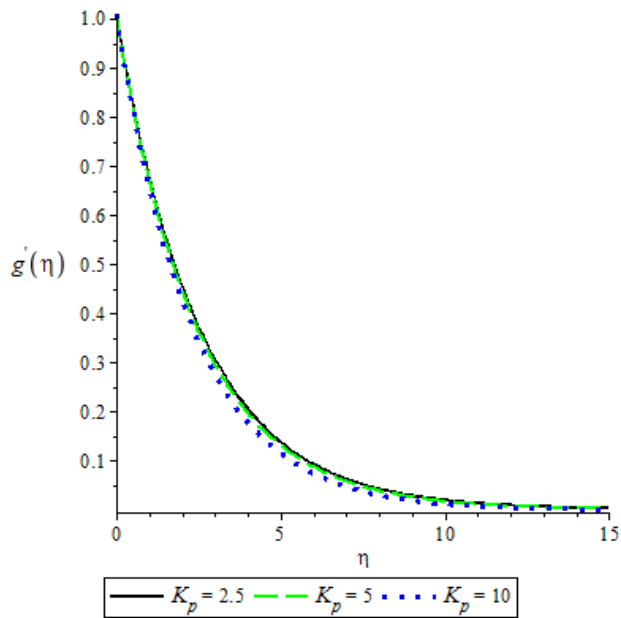
Figure 4.9: Effect of K_p on Velocity Profile $g'(\eta)$
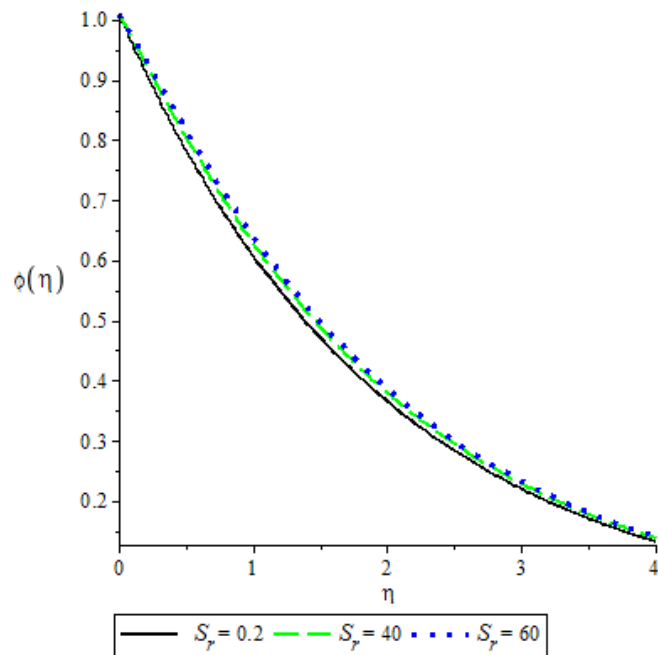
Figure 4.10: Effect of S_r on Concentration Profile $\phi(\eta)$
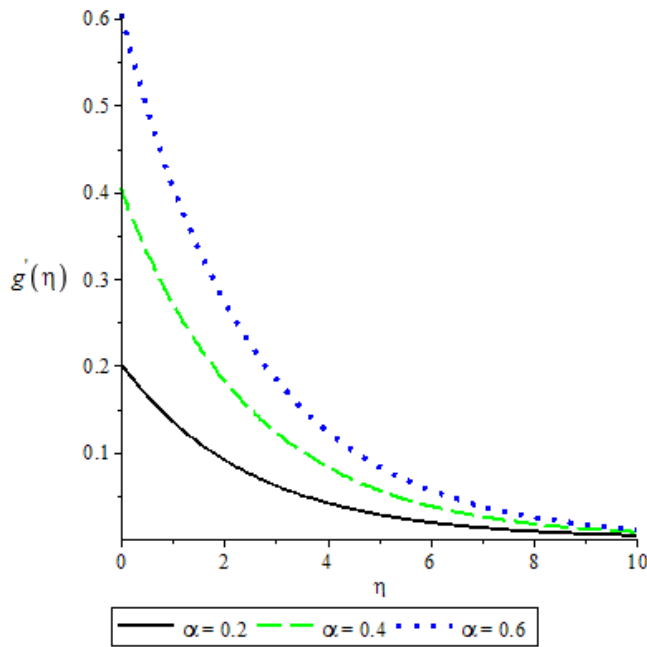
Figure 4.11: Effect of α on Velocity Profile $g'(\eta)$
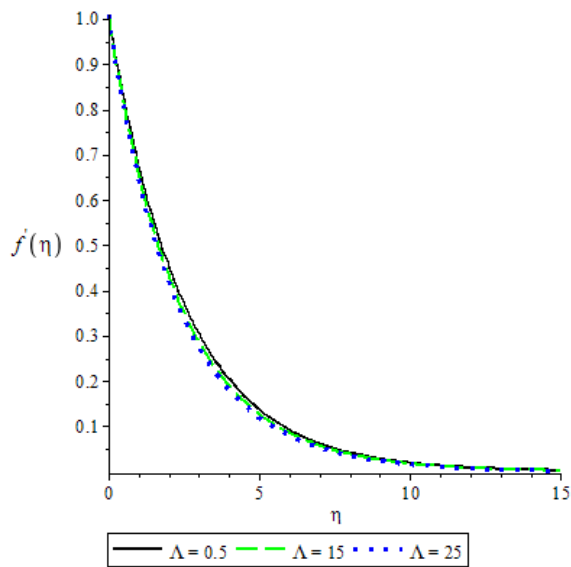
Figure 4.12: Effect of Λ on Velocity Profile $f'(\eta)$
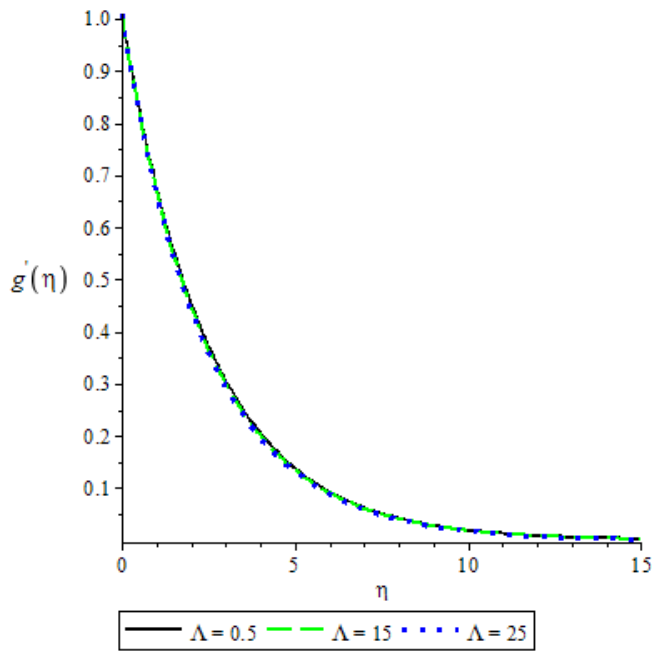
Figure 4.13: Effect of Λ on Velocity Profile $g'(\eta)$
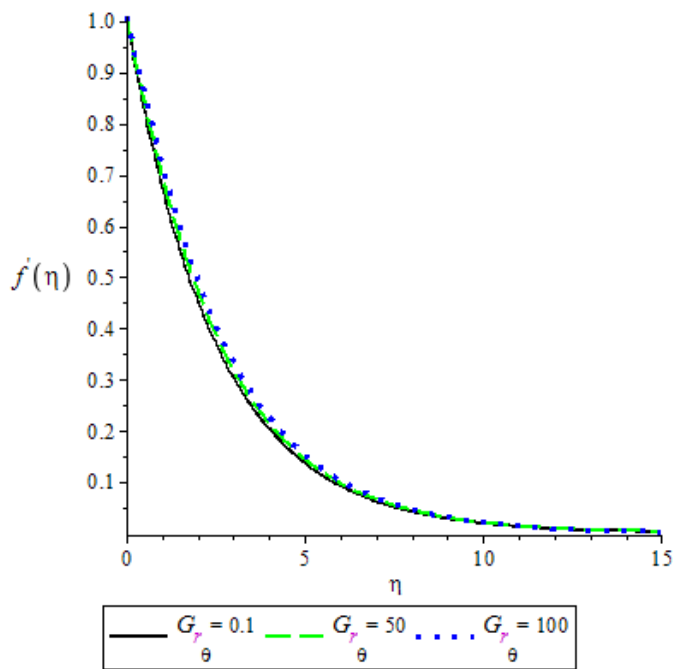
Figure 4.14: Effect of G_{r_θ} on Velocity Profile $f'(\eta)$
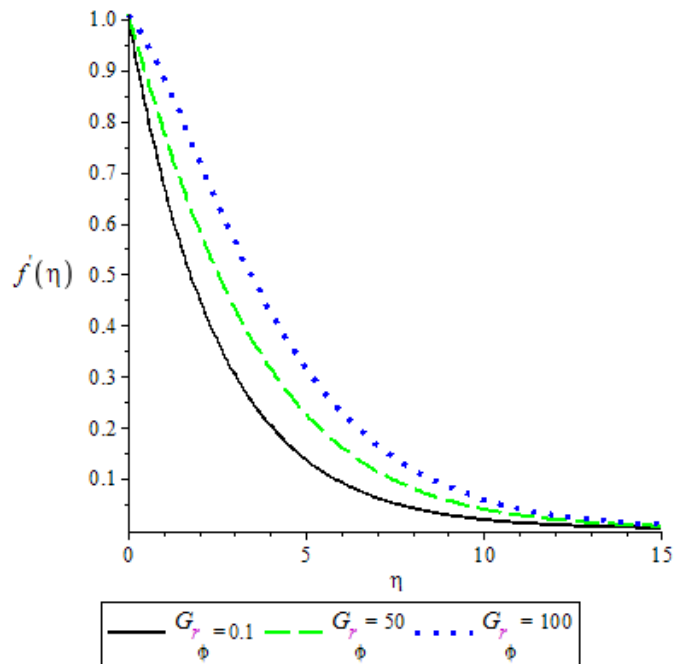
Figure 4.15: Effect of G_{r_ϕ} on Velocity Profile $f'(\eta)$
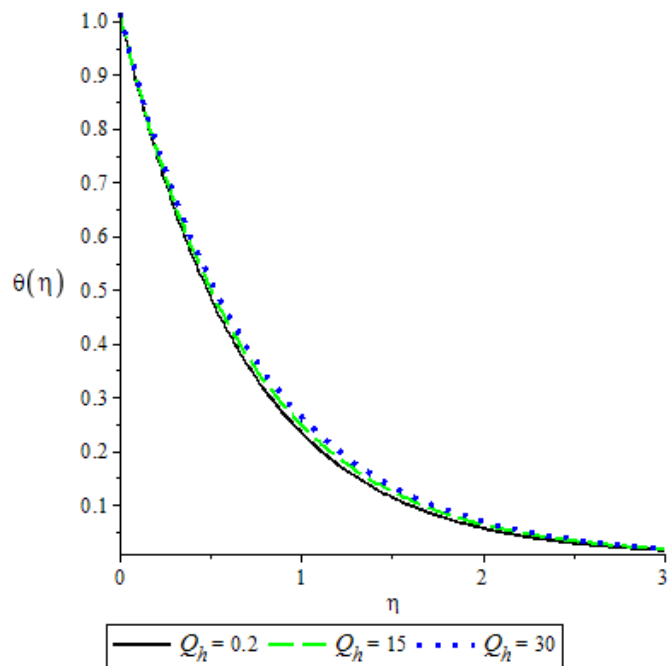
Figure 4.16: Effect of Q_h on Temperature Profile $\theta(\eta)$
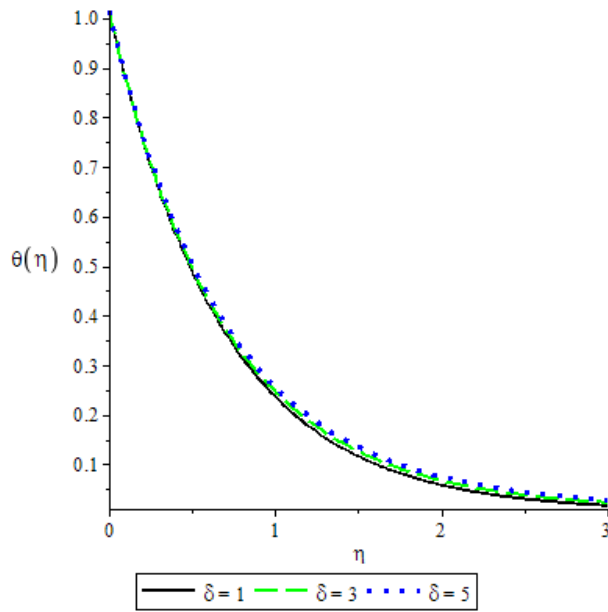
Figure 4.17: Effect of δ on Temperature Profile $\theta(\eta)$
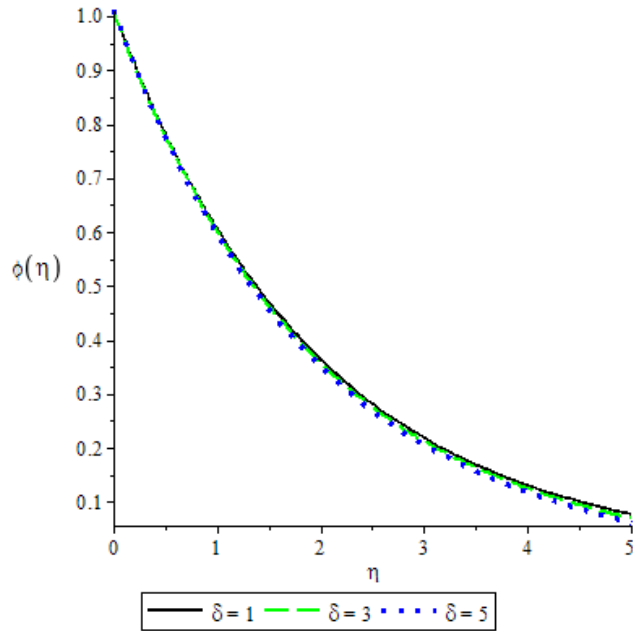
Figure 4.18: Effect of δ on Concentration Profile $\phi(\eta)$
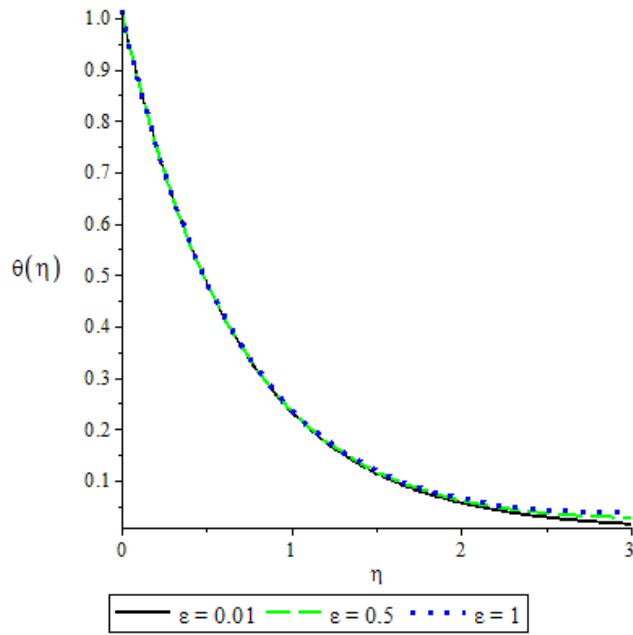
Figure 4.19: Effect of ξ on Temperature Profile $\theta(\eta)$
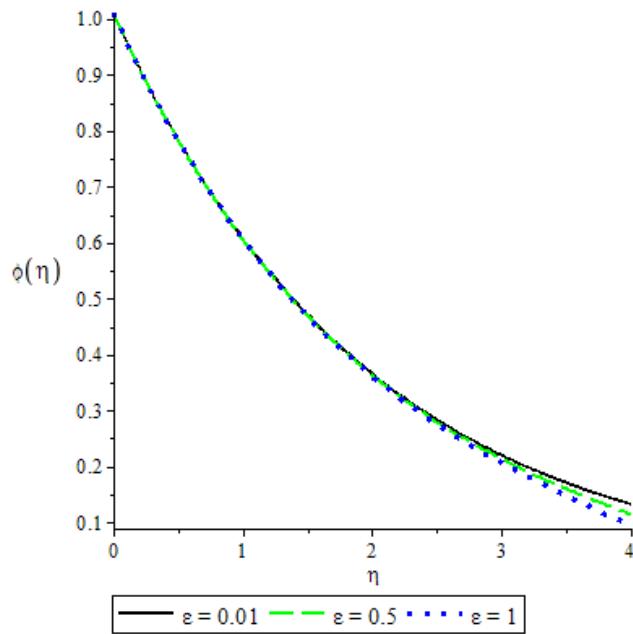
Figure 4.20: Effect of ξ on Concentration profile $\phi(\eta)$
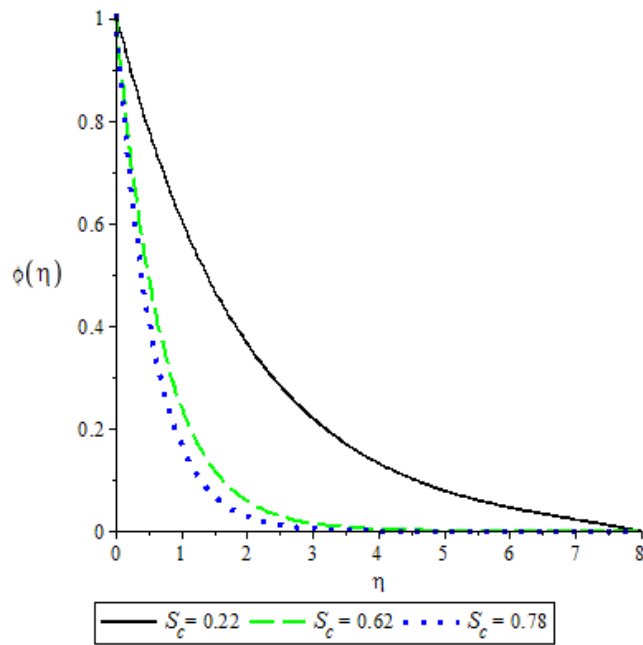
Figure 4.21: Effect of S_c on Concentration Profile $\phi(\eta)$
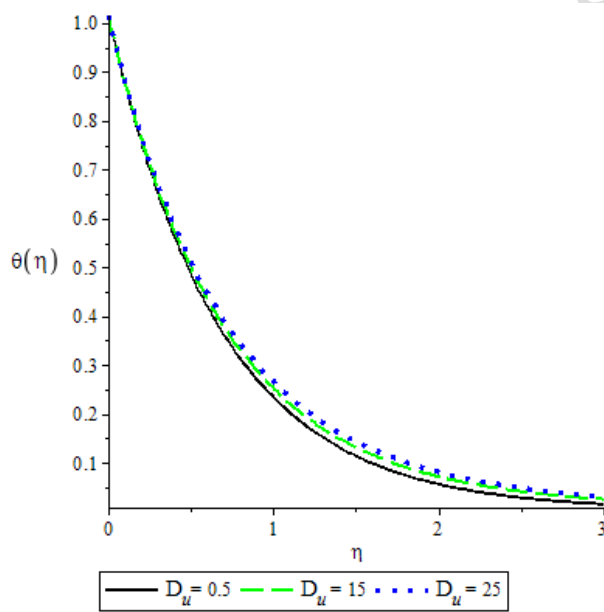
Figure 4.22: Effect of D_u on Temperature Profile $\theta(\eta)$

Figures 4.1 and 4.2 depict the velocity profiles against the similarity variable η for different values of casson parameter β. It was observed from these figures that as casson parameter increases, the fluid velocity distribution decreases

inside the boundary layer. Figures 4.3 and 4.4 show the effects of radiation parameter R and prandtl number P_r on the temperature profile. It was observed that increase in radiation parameter increases the temperature profile while increase in prandtl number decreases the temperature profile. In figures 4.5 to 4.7, it was observed that increase in magnetic parameter decreases the velocity profiles and enhance the temperature profile as shown in figure 4.7. From figures 4.8, 4.9, 4.11, 4.12 and 4.13 to 4.15, we observed that increase in porosity parameter and permeability parameter lead to decrease in velocity profiles, ratio parameter enhances the velocity profile similarly increase in thermal and solutal grashof numbers enhances the velocity profile due to thermal and solutal buoyancy effects while soret number enhances the concentration profile as depicted in figure 4.10. From figures 4.16 to 4.22 shows that increase in heat source parameter, chemical reaction parameter, activation energy parameter and dufour number enhances the temperature profile while chemical reaction parameter, activation energy parameter and schmidtl number decrease the concentration profile.

Conclusion
From the graphical illustrations above we conclude as follows:
- ➢ Ratio parameter, thermal and solutal grashof numbers enhance the velocity profiles while velocity profile decreases with increase in casson, magnetic, permeability and porosity parameters
- ➢ Chemical reaction parameter, activation energy parameter and schmidtl number decrease the concentration profile while Soret number enhance the concentration profile
- ➢ Prandtl number decreases the temperature profile while magnetic parameter, radiative parameter, heat source, dufour number, chemical reaction and activation energy parameters enhance the temperature profile.

References
Charankumar, G., Dharmaiah, G., Balamurugan, K.S. and Vedavathi, N. (2016). Chemical Reaction and Soret Effects on Casson MHD Fluid Flow Over a Vertical Plate, *Int. J. Chem. Sci, 14(1),* 213-221.

Hussainan, Abid., Salleh, Zuki Mohd and Khan Ilyas (2016). Effects of Newtonian Heating and Inclined Magnetic Field on Two Dimensional Flow of a Casson Fluid Over a Stretching Sheet, *5th World Conference On Applied Science, Engineering and Technology HCMUT*, ISBN 13: 978-81-930222-2-1, Pp 251-255.

Kirubhashankar, C. K., Ganesh, S. and Ismail, Mohamed A. (2015). Casson Fluid Flow and Heat Transfer Over an Unsteady Porous Stretching Surface. *Applied Mathematical Science, 9(7),* 345-351.

Kumar, Prasanna T. and Gangadhar, K. (2015), Moment and Thermal Slip Flow of MHD Casson Fluid Over a Stretching Sheet With Viscous Dissipation, *International Journal of Modern Engineering Research(IJMER): 5(5),* ISBN 2249-6645.

Kushapala, K., Reddy, Ramana. J.V., Sugunamma, V. and Sandeep, N. (2017). Numerical Study of Chemically Reacting Unsteady Casson Fluid Flow Past a Stretching Surface With Cross Diffusion and Thermal Radiation. *Open Engineering.*7:69-76.

Maleque, Abdul Kh. (2013). Effects of Exorthermic/Endothermic Chemical Reaction With Arrhenius Activation Energy on MHD Free Convection and Mass Transfer Flow in Presence of Thermal Radiation. *Journal of Thermodynamics.*

Maleque, Abdul Kh. (2016). MHD Non-Newtonian Casson Fluid Heat and Mass Transfer Flow With Exorthermic/Endothermic Binary Chemical Reaction and Activation Energy. *Columbia International Publishing American Journal of Heat and Mass Transfer*, 3, 166-185.

Mohammed, A. A., Olayiwola, R. O and Yisa, E. M. (2015). Simulation of Heat and Mass Mransfer in the Flow of Incompressible Viscous Fluid Past an Infinite Vertical   Plate. *Gen. Math. Notes, ICSRS Publicatiom, Vol.* 31, *pp.* 54-65, *ISSN* 2219- 7184.

Mohammed, I. B. S, Saidu, Yakubu Vulegbo, Olayiwola, R.O and Abubakar, A.D. (2020). Magnetohydrodynamic Casson Fluid Flow Over an Exponential Stretching Sheet with Effect of Radiation, *International journal of pure and applied Science (IJPAS). P-ISSN 139-8466, Vol 12 No 9, 66-80.*

Olayiwola, R. O. (2016). Modeling and Analytical Simulation of A Laminar Premixed Flame Impinging on a Normal Solid Surface. *Nigerian Journal of Mathematics and Applications (NJMA), 25, 226 – 240.*

Parakash, J., Durga, Prasad., Kumar, Vinod. G. Kumar, Kiran. R. V. M. S. S. and Varima, S.   V.   K. (2016). Heat and Mass Transfer Hydromagnetic Radiative Casson Fluid Flow   Over   an Exponentially Stretching Sheet With Heat Source/Sink. *International   Journal of Advanced Science and Technology, 91, 19-38.*

Pushpalata, K., Sugunamma, J. V., Reddy, Ramana and Sadeep, N. (2016). Heat and Mass Transfer in Unsteady MHD Casson Fluid Flow With Convective Boundary Conditions. I*nternational Journal of Advanced Science and Technology,* 91, 19-38.

Saidulu, N and Lakshmi, A. Venkata (2016). Slip Effects on MHD Flow of Casson Fluid Over an Exponentially Stretching Sheet in Presence of Thermal Radiation, Heat Source/Sink and Chemical Reaction. *International Journal of Advanced in Engineering and Technology,* 3(1), 47-55.

Sarojamma, G., Vasundahara, B., and Vendabai, K (2014). MHD Casson Fluid Flow, Heat and Mass Transfer in a Vertical Channel With Stretching Walls. *International Journal of Scientific Innovative Mathematical Research (IJSIMR),* 2, 800-810.

Vedavathi, N., Dharmaiah, G., Balamurugan, K. S. and Kumar, Charan G. (2016). Chemical Reaction Radiation and Dufour Effects on Cassn Magneto Hydro Dynamics Fluid Flow Over a Vertical Plate With Heat Source/Sink. *Global Journal   Of Pure And Applied Mathematics, 12(1),191-200.*